Journal of Organometallic Chemistry 823 (2016) 76–82

Contents lists available at ScienceDirect

Journal of Organometallic Chemistry

journal homepage: www.elsevier.com/locate/jorganchem

Preparation of a novel homogeneous bimetallic Rhodium/Palladium ionic catalyst and its application for the catalytic hydrogenation of nitrile butadiene rubber

Wei Zhou, Xiaohong Peng*

Department of Polymer Science and Engineering, South China University of Technology, Guangzhou, China

ARTICLE INFO

Article history:
Received 29 July 2016
Received in revised form
6 September 2016
Accepted 12 September 2016
Available online 15 September 2016

Keywords:
Poly(propylene imine) dendrimer
Catalytic hydrogenation
Bimetallic ions
Nitrile-butadiene rubber

ABSTRACT

A new hybrid second-generation poly (propylene imine) dendrimer terminated by nitrogen-containing triolefinic macrocycle on the periphery (G2-M) was synthesized. The bimetallic Rhodium (III)/Palladium (II) (Rh^{3+}/Pd^{2+}) dendrimer-stabilized catalysts (G2-M($Rh^{3+}{}_xPd^{2+}{}_{10-x}$)) were prepared by a co-complexation route within G2-M and analyzed by ^1H NMR, XRD and XPS. The catalytic activity, selectivity and separation capability for the hydrogenation of nitrile-butadiene rubber (NBR) catalyzed by the G2-M($Rh^{3+}{}_xPd^{2+}{}_{10-x}$) have been researched. As a novel catalyst system, the bimetallic ions of Rh^{3+} and Pd^{2+} have influenced on the catalytic activity for the hydrogenation of NBR, which can be related to electron-deficiency effect of Rh^{3+} resulting from the interaction of Rh^{3+} and Pd^{2+} within G2-M.

1. Introduction

The copolymer of nitrile-butadiene rubber (NBR) has been widely applied in various fields. However, the residual unsaturated carbon-carbon bonds make NBR susceptible to degradation when exposed to oxygen, ozone, ultraviolet light, high temperature and some other extreme conditions [1,2]. Normally, this deficiency can be alleviated by selectively hydrogenating NBR to yield hydrogenated nitrile-butadiene rubber (HNBR) [3,4].

At present, the solution hydrogenation of NBR has been the main approach of preparing HNBR by using a homogeneous or heterogeneous catalyst. To contrast the difference between using the two catalysts, the former displays higher catalytic activity. Generally, the Rhodium (Rh) and Palladium (Pd) catalysts are the frequently adopted ones for the homogeneous catalytic hydrogenation of NBR [5–10]. Particularly, the Rh catalysts are the most popular homogeneous catalysts because they can provide excellent hydrogenation degree without reduction of nitrile group [11]. However, the high cost results from the high-price of Rh compared with other metals for hydrogenation, such as Pd, and the poor separation of the catalysts from substrates have been the major obstacles. The levels of the metal residues reported are about 160–800 ppm for HNBR before post treatment, which will result in high producing cost of HNBR. Moreover, the large amount of Rh residue can result in crosslinking after hydrogenation [12]. Although the ion extraction, organic extraction and chemical precipitation methods have been applied to reduce the Rh residue, the removal of Rh residue is very time-consuming and costly. Therefore, the preparation of an active bimetallic catalyst, which is consisted of Rh and Pd and can be facilely separated, will be very promising.

Dendritic polymer has a stereoregular, highly branched and well-defined structure. Therefore, the dendrimer-stabilized metallic particles can be obtained by transferring the catalytic active centers to the periphery of the functional dendrimer [13,14]. The peripherally modified dendrimer can stabilize the metallic particles, enhance the catalytic activity, and be easy to remove or recycle. The double bonds in the nitrogen-containing 15-membered triolefinic macrocyclic ligands are excellent electron donators for the transition metallic atoms, and the macrocyclic ligands have high antioxide stabilization and tend to coordinate with metallic atoms to form complexes, which are beneficial to stabilize and recover metals [15,16]. One can see that it might be applicable for the catalytic reaction of polymer substrate. However, few reports have been made on the macrocyclic complexes in a process for the catalytic hydrogenation of NBR.

* Corresponding author.
E-mail address: renewable_2008@126.com (X. Peng).

http://dx.doi.org/10.1016/j.jorganchem.2016.09.009
0022-328X/

In this paper, the hybrid poly (propylene imine) dendrimer (G2-M) has been obtained by modifying the surface of the second-generation PPI dendrimer with 15-membered triolefinic macrocycles. Pd^{2+} was employed to partly replace Rh^{3+} in the preparation of the novel Rh^{3+}/Pd^{2+} catalysts (G2-M($Rh^{3+}{}_xPd^{2+}{}_{10-x}$)). Furthermore, the structure and catalytic activity of the bimetallic Rh^{3+}/Pd^{2+} catalysts were also investigated.

2. Experimental

2.1. Materials

The second-generation poly (propylene imine) dendrimer (G2-PPI) with a diaminobutane core were purchased from SyMO-Chem B. V. in Netherland. The nitrogen-containing triolefinic macrocycle (MAC) poly (propylene imine) and the dendrimer modified by MAC (G2-M) were synthesized by the pathway shown in Scheme 1 and Scheme 2, respectively. $RhCl_3.3H_2O$ (99%) and $Pd(OAc)_2$ (99%) and triphenyl phosphate (TPP, 99%) were purchased from Macklin company (China). NBR (N31, ACN: 33.5 wt%) was obtained from Shanghai Nessen International Trading Company.

The triolefinic 15-membered macrocycle **6** (MAC) has been obtained in excellent yields. For the preparation of **5** the NH_2 groups must be protected in **1** and **2** to avoid *N*-dialkylation in step III, and to obtain a successful reaction between **2** and the arenesulfonamide **2** (step IV).

Scheme 1. Conditions: I. (1) HSO_3Cl, 0 °C (2) $NH_3{\cdot}H_2O$, 13 °C; Yield: 33.4%; II. $(tert\text{-}BuOCO)_2O$, Et_3N, dimethylaminopyridine (DMAP, 0.1 equiv), CH_2Cl_2; Yield: 92%; III. K_2CO_3, CH_3CN, *trans*-1,4-dibromo-2-butene (4 equiv), reflux; Yield: 82.1%; IV. K_2CO_3, CH_3CN, arenesulfonamide (0.5 equiv), reflux; Yield: 67.5%; V. Trifluoroacetic anhydride (TFAA), CH_2Cl_2, room temperature; Yield: 89.3%; VI. K_2CO_3, refluxing CH_3CN, *trans*-1, 4-dibromo-2-butene (1 equiv); Yield: 76.5%.

Characterization data of the arenesulfonamide 3: m. p.: 102 °C; elemental analyses: found C, 39.02; H, 4.27; N, 4.96; S, 11.76. Calc. for $C_9H_{12}BrNSO_2$: C, 38.85; H, 4.32; N, 5.04; S, 11.51. MALDI-TOF MS (matrix alpha-Cyano-4-hydroxycinnamic acid): *m*/*z* Calc. for $C_9H_{12}BrNSO_2$, 278 [M^+]; found, 302.4 [M^+ Na^+]. IR (KBr) 3358, 3273, 2930, 2851, 1595, 1550, 1329, 1168, 902 cm^{-1}.^{1}H NMR (D-DMSO, 600 MHz, ppm): $\delta = 1.28$ (m, 2H), $\delta = 1.95$ (t, 2H), $\delta = 2.68$ (m, 2H), $\delta = 6.48$ (s, 2H), $\delta = 6.59$ (d, $J = 8.8$ Hz, 2H), $\delta = 6.92$ (d, $J = 8.8$ Hz, 2H).

Characterization data of the azamacrocycle 6: m. p.: 139 °C; elemental analyses: found C, 61.13; H, 7.38; N, 4.17; S, 9.27. Calc. for $C_{51}H_{74}BrN_3S_3O_6$: C, 61.20; H, 7.40; N, 4.20; S, 9.60. MALDI-TOF MS (matrix alpha-Cyano-4-hydroxycinnamic acid): *m*/*z* Calc. for $C_{51}H_{74}BrN_3S_3O_6$, 1000 [M^+]; found, 1024.4 [M^+ Na^+]. IR (KBr) 2955, 2858, 1595, 1313, 1155, 972 cm^{-1}. ^{1}HNMR ($CDCl_3$, 600 MHz, ppm): $\delta = 1.24$ (m, 36H), $\delta = 2.18$ (t, 2H), $\delta = 2.87$ (m, 4H), $\delta = 3.39$ (t, 2H), $\delta = 3.78$ (m, 12H), $\delta = 4.08$ (m, 4H), $\delta = 5.77$ (m, 6H), $\delta = 7.15$ (d, 4H), $\delta = 7.36$ (d, $J = 8.8$ Hz, 2H), $\delta = 7.74$ (d, $J = 8.8$ Hz, 2H).

2.2. Preparation of G2-M

MAC (0.48 g, 4.8×10^{-1} mmol) was reacted with G2-PPI (0.052 g, 6.7×10^{-2} mmol) using K_2CO_3 (0.33 g) as an acid-trap in CH_3CN (30 ml) at 82 °C for 24 h under N_2. The crude product was obtained by filtration and rotary evaporation. Finally, the product was washed with ethyl acetate-pentane (1:6) twice to remove the unreacted MAC and dried to obtain pure G2-M as light yellow powdery solid. The preparation route of G2-M is shown in Scheme 2.

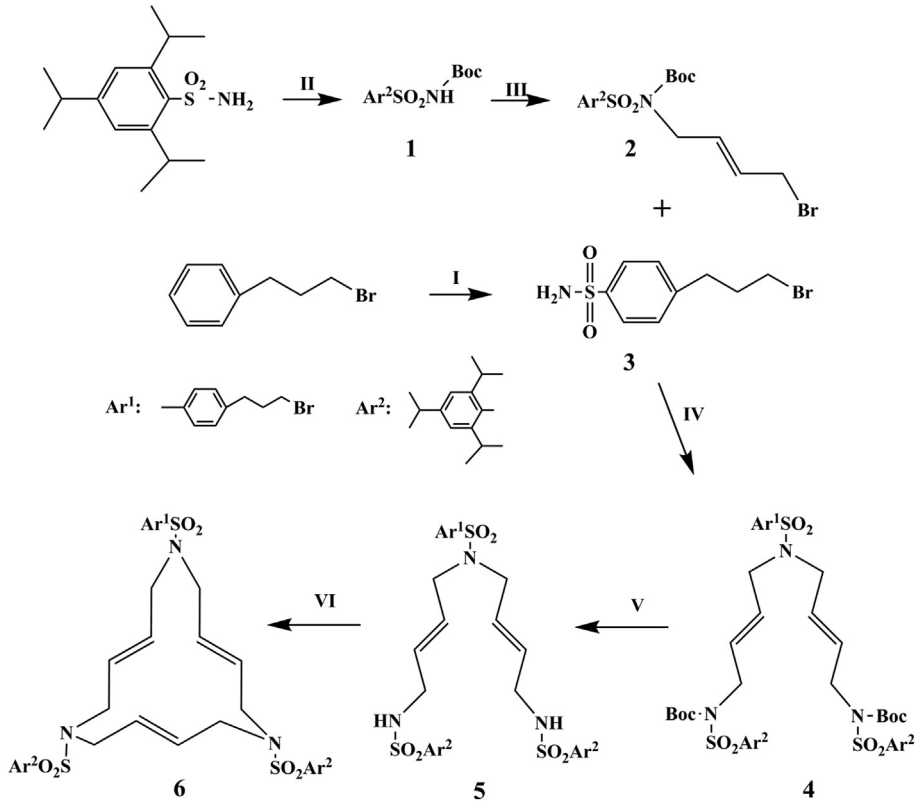

Scheme 1. The synthetic route of MAC.

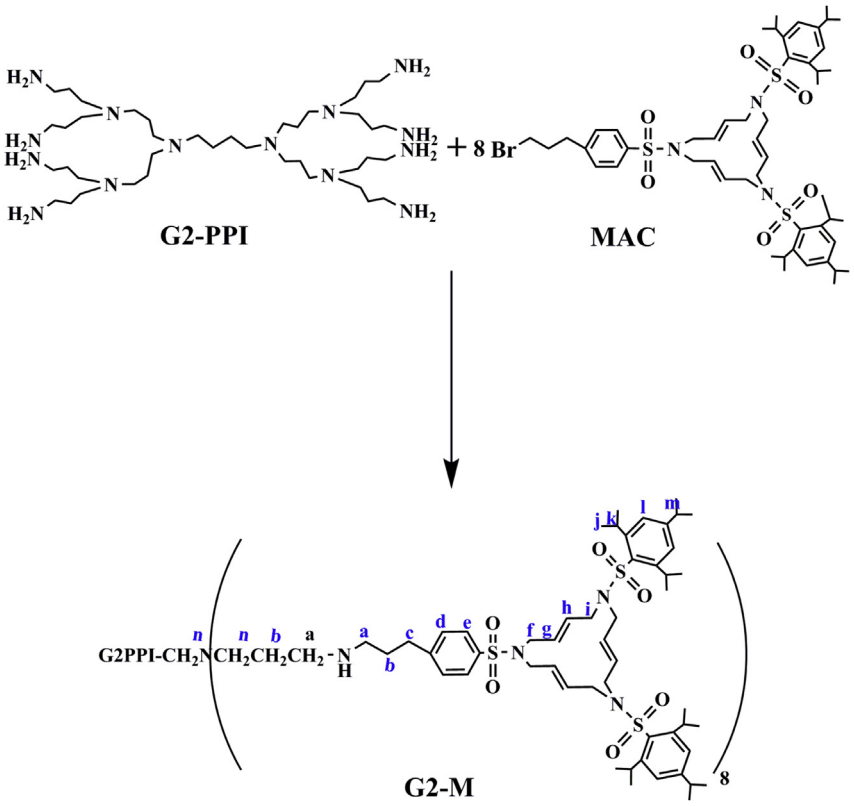

Scheme 2. The synthetic route of G2-M.

2.3. Preparation of G2-M($Rh^{3+}_{x}Pd^{2+}_{10-x}$)

A equivalent mixture of G2-M, and metal complexes of the $RhCl_3 \cdot 3H_2O$ and $Pd(OAc)_2$ (Rh: Pd = 10:0, 7:3, 5:5, 0:10 (mol:mol)) in tetrahydrofuran (20 ml) was stirring for 24 h at room temperature under nitrogen. Then the solvent was removed under reduced pressure to afford solid G2-M($Rh^{3+}_{x}Pd^{2+}_{10-x}$)(see Scheme 3).

2.4. Hydrogenation of NBR

The hydrogenation of NBR was carried out in an autoclave reactor. A certain amount of NBR (0.9 g) dissolved in the monochlorobenzene (35 mL) was first added to the reactor, and then G2-M($Rh^{3+}_{x}Pd^{2+}_{10-x}$) (catalyst/NBR = 0.020–0.022 wt%) was added to the NBR solution. Thereafter H_2 was introduced to the reactor by a hydrogen adapter and maintained at 5.5 MPa after the NBR mixture was degassed with H_2 for three times. The hydrogenation temperature at 100 °C and the stirring speed of 600 rpm were maintained for 7 h. The system was cooled down after a given reaction time. HNBR was obtained by unloading the crude product, adding ethanol to flocculate and drying the filtrated rubber. The organic solution was evaporated, and the G2-M($Rh^{3+}_{x}Pd^{2+}_{10-x}$) was recovered.

2.5. Characterization

The Fourier Transform Infrared Spectra (FT-IR) and Attenuated Total Reflection Infrared Spectra (ATR-IR) were collected by Bruker VERTEX70 Infrared Spectroscopy. The G2-M and G2-M($Rh^{3+}_{x}Pd^{2+}_{10-x}$) were determined by Proton Nuclear Magnetic Resonance (^{1}H- NMR, Bruker Advance III-HD, 600 MHz, $CDCl_3$). The elemental analysis was carried out with Vario EL III organic element analyzer. The Matrix Assisted Laser Desorption Ionization Time of Flight Mass Spectrometry (MALDI-TOF MS) tests were carried out with Autoflex III smartbean mass spectrometer. The X-ray photoelectron spectroscopy (XPS) was measured with an X-ray

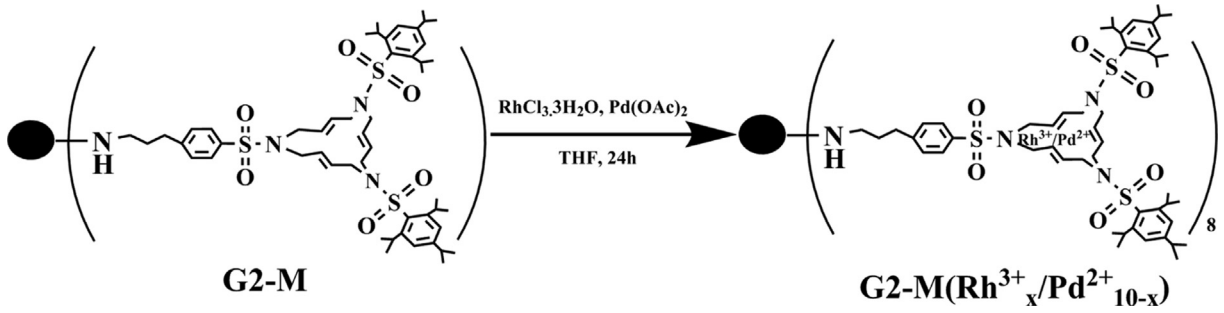

Scheme 3. The preparation of G2-M($Rh^{3+}_{x}Pd^{2+}_{10-x}$).

photoelectron spectrometer (Kratos Axis Ulra DLD). The XRD spectra were collected by an X-ray diffractometer (D8 ADVANCE). The Rh and Pd residues were measured by an atomic absorption spectrometer (Z-2000). The hydrogenation degree X is obtained:

$$X = 1 - [A'_{970+917}/A'_{2236}]/[A_{970+918}/A_{2236}]$$

where the absorption peaks at 2236 cm^{-1}, 970 cm^{-1} and 917 cm^{-1} 723 cm^{-1}correspond to the −C≡N, *trans*-CH═CH and −CH═CH_2 groups in NBR, respectively, A′ is the area sum of the corresponding the peaks of HNBR in FT-IR spectra, and A is the area sum of the peak of NBR in FT-IR spectra.

3. Results and discussion

3.1. Characterization of G2-M

Fig. 1 shows the FT-IR absorption spectra of G2-PPI, MAC and G2-M. As shown in Fig. 1, the absorption bands at 3380 cm^{-1}, 1604 cm^{-1} and 1329 cm^{-1} respectively ascribed to −NH−, -C═C- and O═S═O groups appear in G2-M with the disappearance of the double peaks at 3285-3350 cm^{-1} ascribed to the $-NH_2$ groups in G2-PPI, which indicates the successful preparation of G2-M. The ^{1}H NMR spectrum of G2-M is illustrated in Fig. 2. As shown in Fig. 2, the peaks of G2-M at 2.4 ppm(n), 1.22−1.26 ppm(j) and 3.75 ppm (f, i) are respectively ascribed to the protons of -N-C$\underline{H}_2$-CH_2-, -C-C$\underline{H}_3$ and N−C$\underline{H}_2$−C═C [14]. And the characteristic absorption peaks at 5.70−5.80 ppm (g, h) ppm and 7.15−7.73 ppm (l, d, e) attributed to the protons of -C-C$\underline{H}$═C$\underline{H}$−C- and aromatic groups are detected in G2-M, respectively [15]. Moreover, the result of elemental analysis for G2-M is shown in Table 1. The test values of C, H, N and S in G2-M are very similar with the calculated ones. And the *m*/*z* of 8145 [M^+ Na^+] for G2-M was found by MALDI-TOF MS (matrix of dihydroxybenzoic acid) analysis, which is identical with the *m*/*z* calculated for G2-M ($C_{448}H_{680}N_{38}S_{24}O_{48}$, 8121 [$M^+$]). Combined with all of the characterization and analyses, it can be confirmed that G2-PPI reacted with MAC the completely.

3.2. Characterization of G2-M($Rh^{3+}{}_xPd^{2+}{}_{10-x}$)

The presence of Rh^{3+} and Pd^{2+} coordination with the endocyclic olefins of the macrocycles can be deduced from the ^{1}H NMR spectra in Fig. 3. The G2-M shows signals for the endocyclic olefinic protons

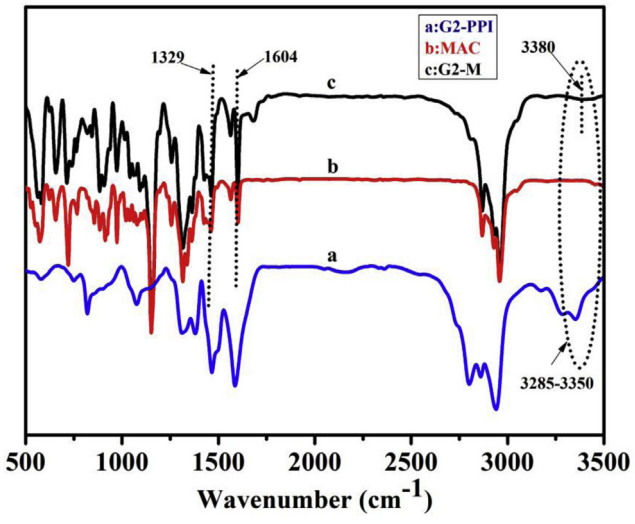

Fig. 1. FT-IR spectra of (a) G2-PPI, (b) MAC, (c) G2-M.

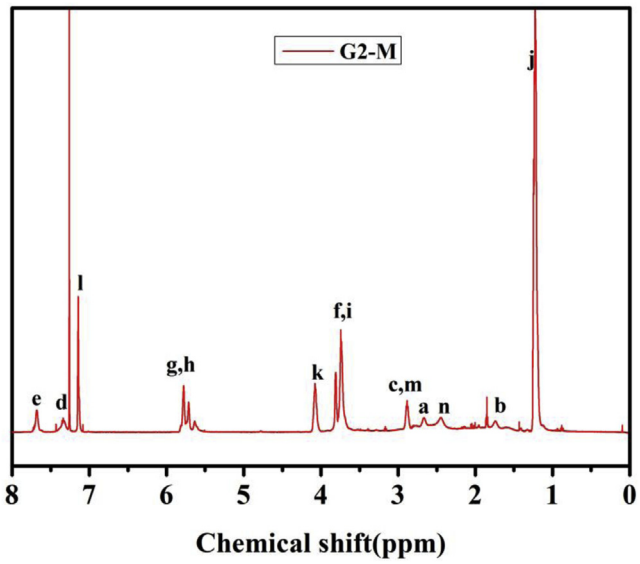

Fig. 2. ^{1}H NMR spectrum of G2-M (600 MHz, $CDCl_3$) δ = 1.22−1.26 (m, 288H, j), δ = 1.54−1.62 (d, 44H, b), δ = 2.40−2.45 (s, 36H, n), δ = 2.63−2.72 (m, 32H, a), δ = 2.87 (m, 32H, c, m), δ = 3.75 (m, 96H, f, i), δ = 4.10 (m, 32H, k), δ = 5.70−5.80 (m, 48H, g, h), δ = 7.15 (d, 32H, l), δ = 7.33 (d, J = 8.8 Hz, 16H, d), δ = 7.70 (d, J = 8.8 Hz, 16H, e).

Table 1
Elemental analysis and calculated values of G2-M.

Element	C		H		N		S	
	Cal./%	Test/%	Cal./%	Test/%	Cal./%	Tes/%	Cal./%	Test/%
G2-M	66.17	65.79	8.37	8.22	6.55	6.61	9.45	9.31

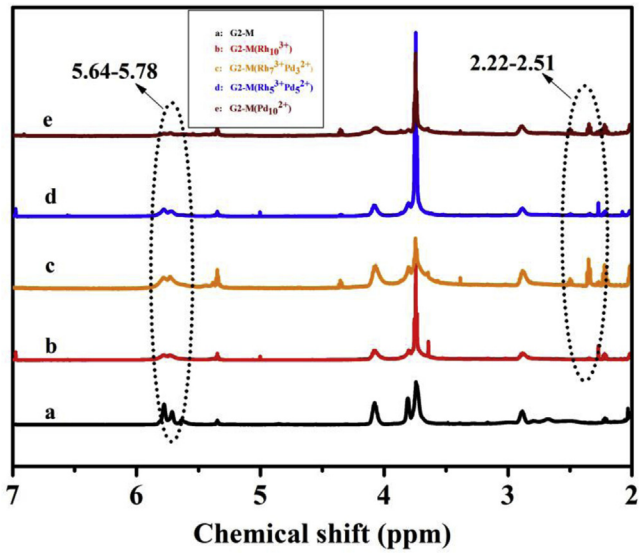

Fig. 3. ^{1}H NMR spectra of G2-M and G2-M($Rh^{3+}{}_xPd^{2+}{}_{10-x}$).

at 5.70−5.80 ppm, whereas the signal intensity at 5.70−5.80 ppm decreases significantly in G2-M($Rh^{3+}{}_xPd^{2+}{}_{10-x}$), and a new up-field shifts at 2.22−2.51 ppm for G2-M($Rh^{3+}{}_xPd^{2+}{}_{10-x}$) is observed, which indicates that macrocycles coordinated with Rh^{3+} and Pd^{2+} successfully.

The XRD patterns of $RhCl_3 \cdot 3H_2O$, $Pd(OAc)_2$, G2-M and G2-M($Rh^{3+}{}_xPd^{2+}{}_{10-x}$) are illustrated in Fig. 4. The characteristic peaks at 9.49°, 36.75°, 52.75° and 65.94° are assignable to

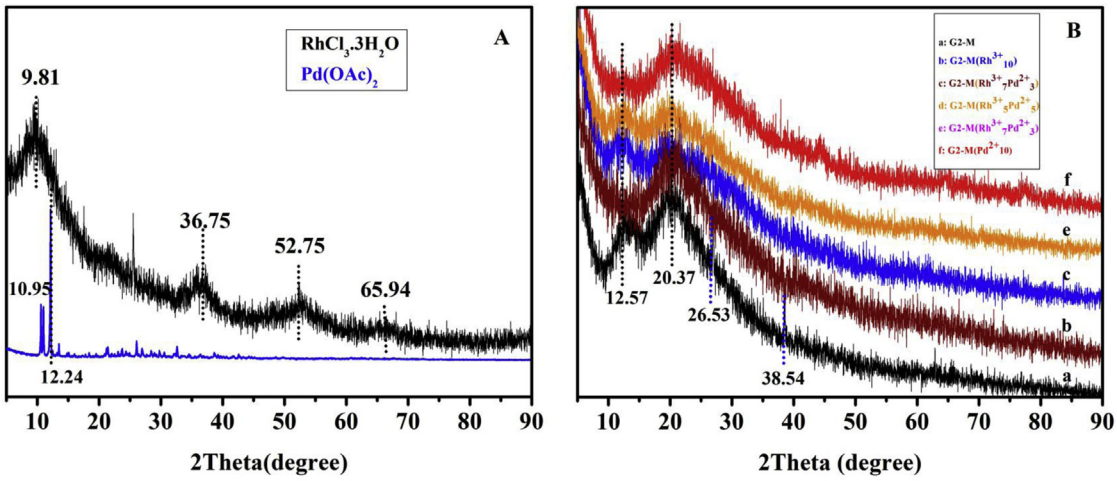

Fig. 4. XRD spectra of $RhCl_3 \cdot 3H_2O$ and $Pd(OAc)_2$(A); G2-M and G2-M($Rh^{3+}_xPd^{2+}_{10-x}$) (B).

$RhCl_3 \cdot 3H_2O$ (Fig. 4A). The characteristic peaks of $Pd(OAc)_2$ are located at 10.95° and 12.24° (Fig. 4A). The G2-M exhibits the characteristic peaks at 12.57°, 20.37°, 26.53° and 38.54° (Fig. 4B). However, after the coordination between macrocycles and the complexes of $RhCl_3 \cdot 3H_2O$ and $Pd(OAc)_2$, the peaks at 26.53° and 38.54° of the macrocycles disappear, and the peaks of G2-M($Rh^{3+}_xPd^{2+}_{10-x}$) at 12.57° and 20.37° of the macrocycles become weaker, indicating the coordination destroyed the crystallinity of G2-M. Moreover, the characteristic peaks of $RhCl_3 \cdot 3H_2O$ and $Pd(OAc)_2$ were not detected in G2-M($Rh^{3+}_xPd^{2+}_{10-x}$) because

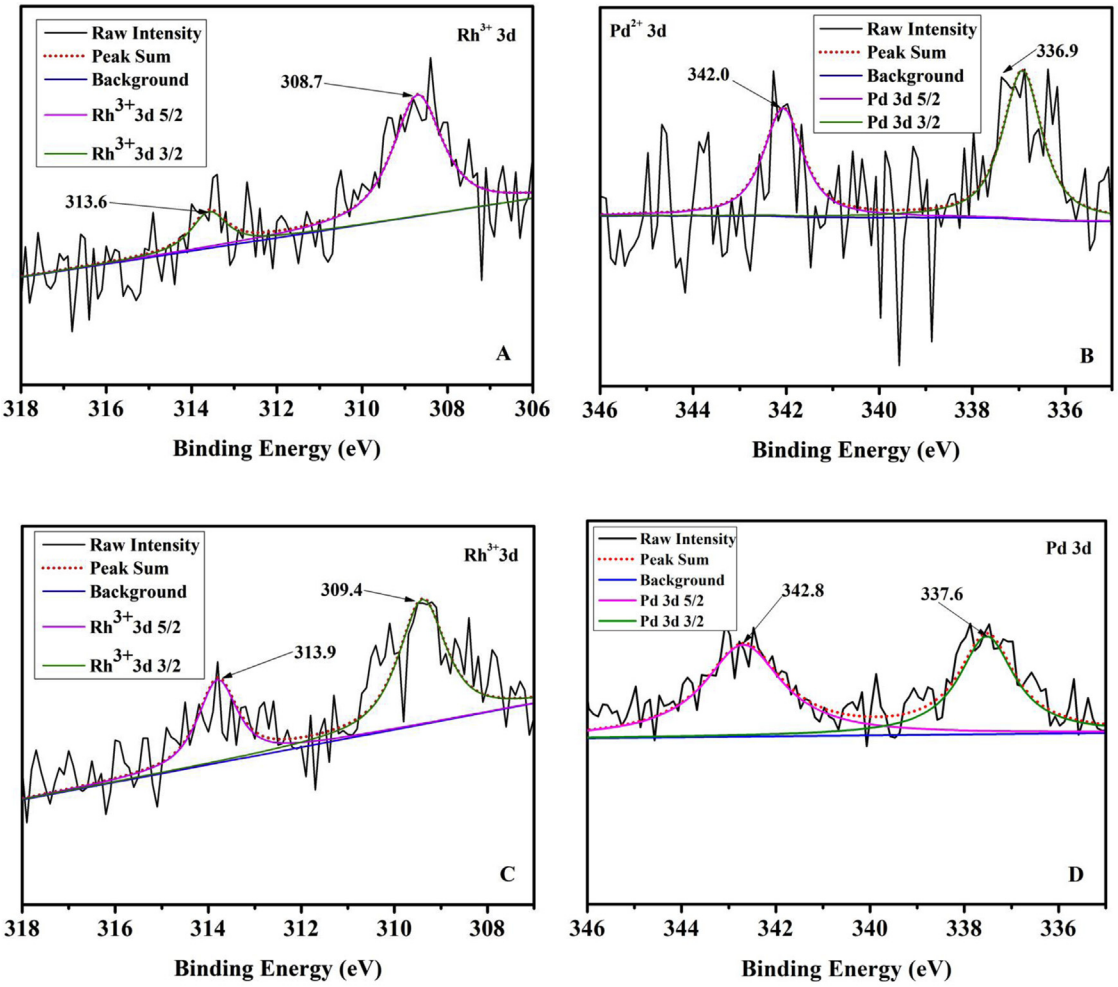

Fig. 5. XPS scans for the G2-M(Rh^{3+}_{10}) (A), G2-M($Rh^{3+}_7Pd^{2+}_3$) (B, C) and G2-M(Pd^{2+}_{10}) (D).

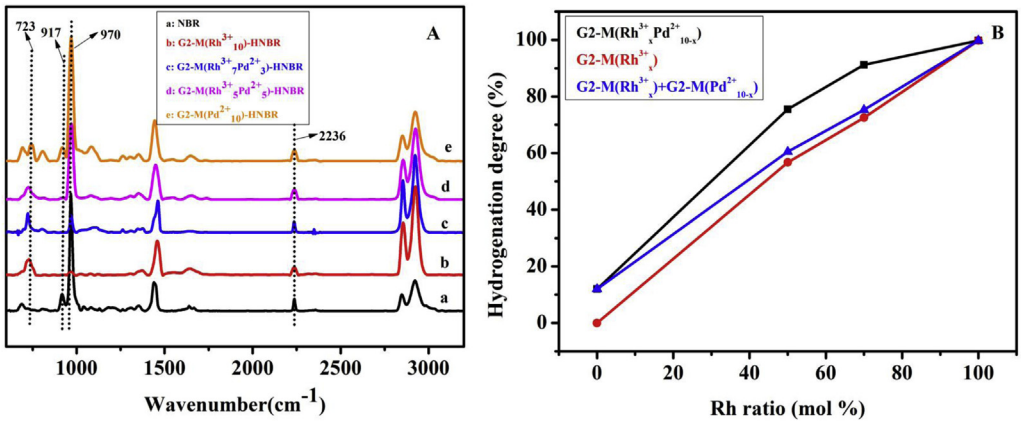

Fig. 6. The FT-IR spectra of HNBR catalyzed by G2-M($Rh^{3+}_xPd^{2+}_{10-x}$) (A); the hydrogenation degrees for HNBR catalyzed by G2-M($Rh^{3+}_xPd^{2+}_{10-x}$), G2-M(Rh^{3+}_x) and the physical mixture of G2-M(Rh^{3+}_x)/G2-M(Pd^{2+}_{10-x}) (B). Reaction condition: catalyst concentration = 0.020 wt%, 100 °C, 600 rpm, 5.5 MPa, 7 h.

of the strong interaction of Rh^{3+} and Pd^{2+} with the cores of the triene heterocycles destroying the crystallinity of $RhCl_3{\cdot}3H_2O$ and $Pd(OAc)_2$.

Fig. 5 presents the XPS scans of the Rh^{3+} and Pd^{2+} binding energy regions for the G2-M(Rh^{3+}_{10}), G2-M($Rh^{3+}_7Pd^{2+}_3$) and G2-M(Pd^{2+}_{10}). The XPS peaks of Rh^{3+} 3d for G2-M(Rh^{3+}_7 Pd^{2+}_3) (Fig. 5C) are present at 309.4 eV ($3d_{5/2}$) and 313.9 eV ($3d_{3/2}$), which are higher than those for Rh^{3+} 3d of G2-M(Rh^{3+}_{10}) (Fig. 5A): 308.7 ($3d_{5/2}$) and 313.5 eV ($3d_{3/2}$), respectively. The XPS peaks of Pd^{2+} 3d for G2-M(Rh^{3+}_7 Pd^{2+}_3) (Fig. 5B) are present at 342.0 eV ($3d_{5/2}$) and 336.9 eV ($3d_{3/2}$), which are lower than those for Pd^{2+} 3d of G2-M(Pd^{2+}_{10}) (Fig. 5D): 342.8 eV ($3d_{5/2}$) and 337.6 eV ($3d_{3/2}$), respectively. The binding energy shifts of Rh^{3+} 3d and Pd^{2+} 3d in G2-M(Rh^{3+}_7 Pd^{2+}_3) may be attributed to the shift of electron density from the Rh^{3+} to the Pd^{2+} within the macrocycles of G2-M.

3.3. Catalytic hydrogenation

Fig. 6A shows the FT-IR spectra of HNBR catalyzed by G2-M($Rh^{3+}_xPd^{2+}_{10-x}$). The absorption peaks at 2236 cm^{-1}, 970 cm^{-1} and 917 cm^{-1} correspond to the −CN, *trans*-CH=CH- and −CH=CH_2 groups of NBR. As shown in Fig. 6A, the absorption $-NH_2$ peak at 3300–3400 cm^{-1} does not appear after the hydrogenation, indicating the excellent selectivity of G2-M($Rh^{3+}_xPd^{2+}_{10-x}$). The relative intensity ($A_{970+918}/A_{2236}$) of the double bond decreases with the Rh^{3+} ratio in G2-M($Rh^{3+}_xPd^{2+}_{10-x}$) increasing, as the Rh^{3+} is a more active catalytic metallic ion than Pd^{2+} [17]. As shown in Fig. 6B, the hydrogenation degrees for HNBR catalyzed by G2-M($Rh^{3+}_xPd^{2+}_{10-x}$) (x = 7, 5) are higher than the ones catalyzed by G2-M(Rh^{3+}_x) (x = 7, 5) and the physical mixture of G2-M(Rh^{3+}_x)/G2-M(Pd^{2+}_{10-x}) (x = 7, 5). This can be ascribed to the more significant electron deficiency of Rh^{3+} resulting from the interaction between Rh^{3+} and Pd^{2+}, which can make the Rh^{3+} more active because the NBR with double bond favors the electron-deficient surface. Although the hydrogenation degree of HNBR catalyzed by G2-M($Rh^{3+}_7Pd^{2+}_3$) (95.5%) was lower than the HNBR catalyzed by G2-M(Rh^{3+}_{10}) (99.8%) when the catalyst concentrations were both 0.020 wt%, the hydrogenation degree of the HNBR catalyzed by G2-M($Rh^{3+}_7Pd^{2+}_3$) could reach 99.9% when the G2-M($Rh^{3+}_7Pd^{2+}_3$) concentration slightly increased to 0.022 wt%.

Importantly, the Rh and Pd residue in HNBR catalyzed by G2-M($Rh^{3+}_7Pd^{2+}_3$) (concentration = 0.022 wt%) were only respectively 17 ppm and 8 ppm without any post treatment, and the recovering rate of G2-M($Rh^{3+}_7Pd^{2+}_3$) could reach as high as 94.1%. As a comparison, the hydrogenation degree for HNBR catalyzed by $RhCl(PPh_3)_3$ (the most popular catalyst for the hydrogenation of NBR, concentration = 0.022 wt%) was only 95.8%, and the Rh residue in HNBR was as high as 265 ppm. The high catalytic capability of G2-M($Rh^{3+}_7Pd^{2+}_3$) compared with the $RhCl(PPh_3)_3$ can be ascribed to the peripheral multi-active centers which can enhance the catalytic activity of the catalyst and the electron-deficiency effect resulting from the interaction of the bimetallic ions of Rh^{3+} and Pd^{2+}. It can also be seen that the strong coordination between G2-M and the bimetallic ions of Rh^{3+} and Pd^{2+} impeded the metals leaching in the hydrogenation process and the favourable solubility of G2-M($Rh^{3+}_7Pd^{2+}_3$) in the co-solvents of ethanol and monochlorobenzene reduced the catalyst encapsulation in HNBR during the separation process.

4. Conclusions

The homogeneous G2-M($Rh^{3+}_xPd^{2+}_{10-x}$) catalysts were prepared by the coordination between G2-M and the complex of $RhCl_3{\cdot}3H_2O$ and $Pd(OAc)_2$. G2-M($Rh^{3+}_xPd^{2+}_{10-x}$) displayed remarkable catalytic activity, high selectivity and facile separation capability for the hydrogenation of NBR. The hydrogenation degree for the HNBR catalyzed by G2-M($Rh^{3+}_7Pd^{2+}_3$) can reach 99.9%.The composition of bimetallic ions influenced on the catalytic activity of G2-M($Rh^{3+}_7Pd^{2+}_3$) because of the electron deficiency effect of Rh^{3+} resulting from the interaction between Rh^{3+} and Pd^{2+}. The metal (Rh and Pd) residue for the HNBR catalyzed by G2-M($Rh^{3+}_7Pd^{2+}_3$) decreased 90.6% compared with the traditional catalyst of $RhCl(PPh_3)_3$. The recovering rate of G2-M($Rh^{3+}_7Pd^{2+}_3$) can reach as high as 94.1% after the first hydrogenation of NBR.

Acknowledgment

This work was supported financially by the National Natural Science Foundation of China (Project No. 51273071).

References

[1] X.Z. Wang, L.Q. Zhang, Y. Han, X.K. Shi, W.M. Wang, D.M. Yue, J. Appl. Polym. Sci. (2013) 4764–4768.
[2] S.M. Ning, S.F. Yang, X.P. Wei, W.M. Wang, L.Q. Zhang, D.M. Yue, J. Appl. Polym. Sci. 123 (2012) 1040–1046.
[3] H. Wang, L.J. Yang, G.L. Rempel, Polym. Rev. 53 (2013) 192–239.
[4] Y. Liu, J.L. Wu, Q.M. Pan, G.L. Rempel, Top. Catal. 55 (2012) 637–643.
[5] G.H. Li, Q.M. Pan, G.L. Rempel, Macromol. Symp. 204 (2003) 141–149.
[6] Q.M. Pan, G.L. Rempel, Macromol. Rapid Commun. 25 (2004) 843–847.
[7] C. Peng, Y.Q. Ni, R. Zou, L.Q. Zhang, D.M. Yue, RSC Adv. 5 (2015) 3417–3424.
[8] J.S. Parent, N.T. McManus, G.L. Rempel, Ind. Eng. Chem. Res. 35 (1996) 4417–4423.

[9] P. Martin, N. McManus, G.L. Rempel, J. Mol. Catal. A Chem. 126 (1997) 115–131.
[10] Q. Pan, G.L. Rempel, Ind. Eng. Chem. Res. 39 (2000) 277–284.
[11] Y. Liu, H. Kim, Q.M. Pan, G.L. Rempel, Catal. Sci. Technol. 3 (2013) 2689–2698.
[12] L.J. Yang, Q.M. Pan, G.L. Rempel, Catal. Today 207 (2013) 153–161.
[13] D. Astruc, E. Boisselier, C. Ornelas, Chem. Rev. 110 (2010) 1857, 1959.
[14] S.A. Samera, M.A.M. Reza, Cellulose 19 (2012) 1701–1714.
[15] E. Badetti, A.M. Caminade, J.P. Majoral, M. Moreno-Mañas, R.M. Sebastián, Langmuir 24 (2008) 2090–2101.
[16] M. Moreno-Mañas, R. Pleixats, R.M. Sebastián, A. Vallribera, A. Roglans, J. Organomet. Chem. 689 (2004) 3669–3684.
[17] Y. Liu, J.L. Wu, Q.M. Pan, G.L. Rempel, Top. Catal. 55 (2012) 637–643.